Magnetic and metal-semiconductor transitions in ordered and disordered $ErH(D)_{2+x}$

P. Vajda
Laboratoire des Solides Irradiés, Centre National de la Recherche Scientifique, Ecole Polytechnique, F-91128 Palaiseau, France

J. N. Daou*
Hydrogène dans les Métaux, Centre National de la Recherche Scientifique, Bâtiment 350, Université Paris-Sud, F-91405 Orsay, France
(Received 27 July 1993)

The electrical resistivity in the system β-$ErH(D)_{2+x}$ was measured in the range $1.3 \leq T \leq 330$ K through the whole region of the pure β phase, $0 \leq x \leq 0.09$. The excess H(D) atoms on octahedral sites, x, adjust for $x \gtrsim 0.05$ first in a short-range order (SRO) and then in a long-range order (LRO) of the H_0 sublattice in the region 150 to 250 K. The activation energies for $H(D)_0$ migration, determined after a quench across the ordering interval, are: E_m(SRO)=0.17(1) eV and E_m(LRO)=0.30(1) eV, without a notable isotope effect. E_m(LRO) decreases slightly with increasing x. A magnetic transition is observed at $T_N=2.32(2)$ K for the pure dihydride ($x=0$); with increasing x, T_N decreases first due to decreasing carrier density, then grows again after the formation of structural LRO, probably because of perturbed crystal-field symmetry. A magnetic phase diagram is proposed using the present data and earlier susceptibility and neutron-diffraction results. The specimens with the highest x concentrations exhibit metal-semiconductor transitions, both at high temperatures (230–290 K) and at low temperatures (40–120 K). The former are related with the order-disorder transformation in the H_0 sublattice, the latter attributed to carrier localization via a Mott mechanism.

I. INTRODUCTION

Like most of the other rare-earth dihydrides, ErH_2 crystallizes in the fluorite structure (β phase) where the two hydrogen atoms occupy ideally both available tetrahedral (T) sites. Additional hydrogens x are inserted on octahedral (O) interstitial sites, up to a limiting concentration, $x^{\beta}_{\max}$, before transforming into the hexagonal trihydride (γ phase). The β phase being metallic and the γ phase semiconducting or insulating, we have, thus, the opportunity to observe a concentration-dependent metal-semiconductor (MS) transition. The β-phase limit decreases generally with increasing atomic number of the rare earth R and is dependent on the metal purity; it is, in the case of β-$ErH(D)_{2+x}$, of the order of $x^{\beta}_{\max} \sim 0.1$ at. %H(D)/at. %Er. A general review of the properties of the R-H systems has been given recently by the present authors.[1] In addition to the x-dependent MS transitions mentioned above, there exist also temperature-dependent MS transitions, which had been first noted near room temperature in the light R hydrides CeH_{2+x} (Ref. 2) and LaH_{2+x} (Ref. 3) for high values of x, $0.7 \lesssim x \lesssim 0.9$, and later in $YH_{2.1}$ (Ref. 4) and $GdH_{2.3}$ (Ref. 5), close to the β-phase limit. A further MS transition (with *decreasing* T) was observed in the two latter systems below ~ 100 K. The high-T transition was attributed to the breakdown of a delocalized carrier band following an order-disorder transformation in the O-hydrogen (H_0) sublattice, the low-T transition to electron localization due to atomic disorder.

In this paper we present complete results of a detailed electrical resistivity study of the β-$ErH(D)_{2+x}$ system prepared from 99.99%-pure Er metal, in the whole solid-solution range $0 \leq x \leq 0.09$ in the interval $1.3 \leq T \leq 330$ K. We observe structural ordering in the octahedral H sublattice for $x \gtrsim 0.05$, concentration-dependent magnetic transitions at low temperatures, and MS transitions at high temperatures; it shall be shown how the atomic ordering interacts with the two electronic transformations. A tentative magnetic phase diagram will conclude the paper.

Earlier work on this system is rather scarce and nonsystematic and concerned mainly with the investigation of the magnetic properties of the pure ($x=0$) erbium dihydride, prepared from—at best—99.9%-pure Er metal and sometimes of much poorer quality. Kubota and Wallace[6] measured the susceptibility in the paramagnetic state. Opyrchal and Bieganski[7] reported a magnetic transition at $T_N=2.13$ K in specific-heat experiments and Shenoy *et al.*[8] at 2.4 K in a Mössbauer experiment. Carlin and Krause[9] noted magnetic ordering in $ErH_{2.08}$ at 2.6 K. Shaked *et al.*[10] had analyzed the magnetic reflections appearing in ErD_2 below $T_N=2.15$ K in a neutron-diffraction study and deduced that the magnetic structure consisted of commensurate and incommensurate components down to at least 1.4 K. The paramagnetic spin-disorder resistivity, ρ_{mag}, of ErH_2 was investigated in electrical resistivity measurements by Daou, Vajda, and Burger[11] and the acoustic and optical vibrations in erbium dihydride and dideuteride by Burger *et al.*[12] Most of these studies indicated a strong influence of crystal-field (CF) effects. Finally, a magnetic-susceptibility investigation made in our laboratory on a series of β-$ErH(D)_{2+x}$ specimens of the same origin and published in a companion paper,[13] will serve as a complementary data source for the construction of the magnetic phase diagram presented here.

II. EXPERIMENT

The specimens were prepared from 99.99 at. % erbium foil of 240-μm thickness purchased from the Ames Laboratory (Ames, Iowa), which contained the stated main metallic impurities (> 1 at. ppm):19 Fe, 6 Pb, 5.2 Dy, 4 Ho, 2.4 Ta, 1.4 Cu; vacuum fusion analysis indicated 250 at. ppm F, 100 C, 60 O, 16 N, and 14 Cl. The foil was degassed at 900 °C in 3×10^{-8} Torr for 20 h, then cut into 20×1 mm^2 strips and provided with four spot-welded platinum leads as contacts. The ensuing hydrogenation occurred in two steps: (i) the preparation of the dihydride by direct absorption in a calibrated volume at 600–650 °C, yielding concentrations of 1.96–1.985 at. %H/at. %Er (the dideuterides were generally of somewhat lower composition: 1.94–1.98 at. %D/at. %Er); (ii) the addition of the excess hydrogens on octahedral sites x at 400–450 °C under an equilibrium pressure. The concentrations were determined by pressure-difference measurements with Baratron high-precision capacitance manometers to ±0.005 at. %H/at. %Er. The final specimens comprised the following x concentrations: in the ErH_{2+x} series, $x=0$, 0.025, 0.03, 0.048, 0.054, 0.07, 0.088, and 0.091 H/Er, in the ErD_{2+x} series, 0, 0.01, 0.04, 0.045, 0.05, 0.08, and twice 0.09 D/Er. Specimens with higher H(D) concentrations already contained some hydrogen in the very unstable γ phase and decomposed in air.

The electrical measurements were performed by the classical dc four-point procedure in a pumped liquid-helium cryostat with temperature regulation. Up to seven specimens were mounted on a sample holder and could be measured simultaneously, reducing the calibration problem and leading to a relative precision of the temperature determination between the samples of $\Delta T<0.05$ K in the magnetically interesting range below ~10 K. Two cooling regimes were applied in order to investigate the influence of eventual x-atom ordering in the O sublattice: (i) relaxed (designated "R" in the presented experimental curves), where the specimens were slowly cooled from room temperature at a rate of ~0.2 K/min and measured, both with decreasing and increasing T; (ii) quenched (designated "Q"), by dipping the sample holder into liquid nitrogen, leading to a cooling rate of $\sim10^3$ K/min and freezing in the room-temperature configuration.

III. RESULTS AND DISCUSSION

A. Structural ordering

In Fig. 1 are presented the temperature dependences of the electrical resistivities of a series of selected ErH_{2+x} specimens to show the typical evolution of their behavior with the concentration x as parameter. Thus, the $x=0$ sample exhibits a resistivity which can be described by a sum of the following terms:

$$\rho(T)=\rho_r+\rho_{\rm mag}(T)+\rho_{\rm ph}(T)\ ,$$

where ρ_r is the residual resistivity, $\rho_{\rm mag}(T)$ is the magnetic spin-scattering term disappearing below T_N (see Sec. III B and Fig. 9 for details), passing through a range

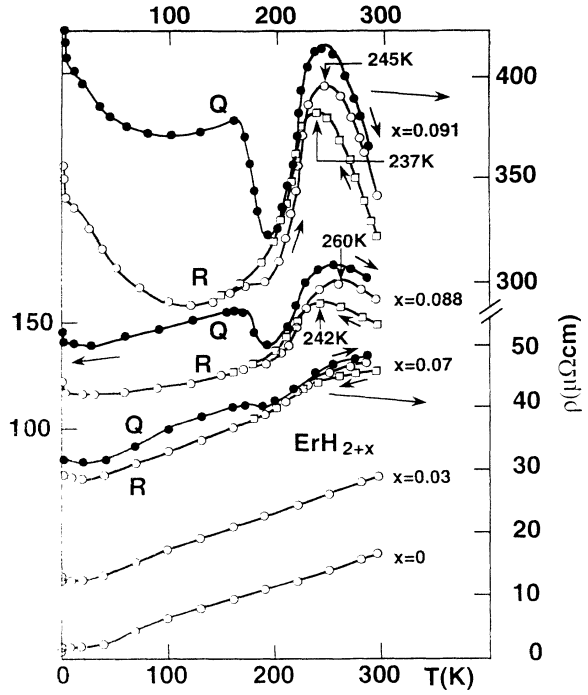

FIG. 1. Resistivity of several ErH_{2+x} specimens, $0\le x\le0.091$, as a function of temperature, showing the MS transitions for high x values. R: slowly cooled (relaxed) state; Q: quenched state. Note the hysteresis around 200 K caused by an order-disorder transformation in the H_0 sublattice, in addition to that around the MS transition.

determined by thermally excited CF-level splitting and attaining a constant value above $T\sim100$ K (it had been analyzed in Ref. 11); $\rho_{\rm ph}(T)$ is the phonon-scattering term superimposed upon $\rho_{\rm mag}(T)$ from $T\sim40$ K on, which can be decomposed in acoustic (or host metal) vibrations and optic (or H sublattice on T sites) vibrations;[12] the growing role in the latter is seen as a slight upturn of $\rho(T)$ when approaching room temperature. The resistivity of the $x=0.03$ sample is rather parallel to that of $x=0$, apart from the appearance of a shallow minimum near 15 K, which we shall discuss in the Sec. III B; it is just shifted upwards by ~12 $\mu\Omega$ cm, corresponding to the increase of ρ_r, and gives a value for the specific resistivity of a x hydrogen atom added on an O site:

$$\Delta\rho^x\sim4\ \mu\Omega\,{\rm cm}\ \text{per at. \%H/at. \%Er in excess}\ .$$

[Compare also the linear $\rho(x)$ dependence for $x<0.07$ in Fig. 8.]

From $x\sim0.05$ on—we show in Fig. 1 the $x=0.07$ specimen as an example—an anomaly appears in the region between 150–200 K, presenting a thermal hysteresis and developing toward a transformation stage with increasing x. The latter exhibits a peak near 250 K indicating a metal-semiconductor transition, which shall be treated in Sec. C below. The resistivity anomaly resembles strongly that observed earlier in other RH_{2+x} systems (for a recent review see, e.g., Ref. 5) and is a sign of a structural order-disorder transformation in the H_0 sublattice. The ordered low-temperature phase had been an-

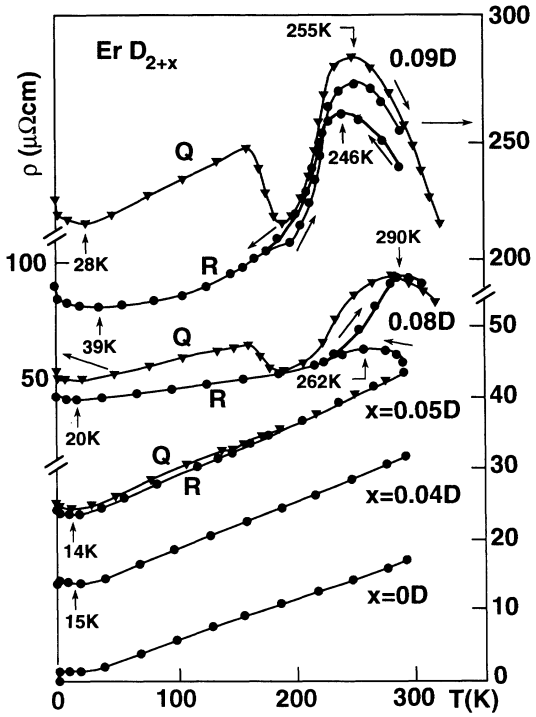

FIG. 2. Same as Fig. 1, in the case of ErD_{2+x} specimens.

alyzed in the case of $\beta-TbD_{2+x}(0.10 \lesssim x \lesssim 0.25)$ by neutron scattering[14] and turned out to be a DO_{22} structure of the Ni_3Mo-type, where the x atoms are ordering in such a way that one occupied (420) plane is followed by three empty ones. Before proceeding to the description of the quenching experiments (indicated as Q in Fig. 1), which are a good testing ground for the ordering kinetics, we shall present, for the sake of completeness, the resistivity data for the corresponding ErD_{2+x}-specimens in Fig. 2. The gross evolution with x is quite analogous to the ErH_{2+x}-samples of Fig. 1, concerning both the appearance of the structural anomaly and the MS transition.

1. *Quenching experiments*

Quenching from room temperature across the ordering region freezes in, at least partially, the disordered state of

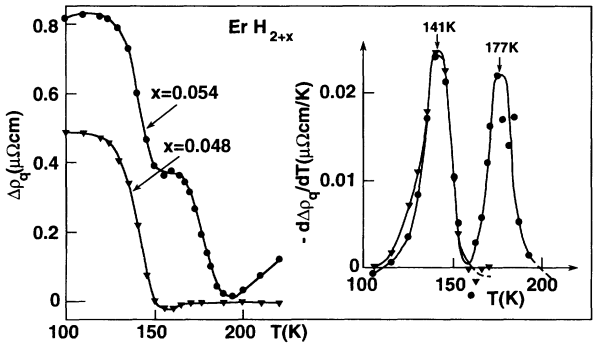

FIG. 3. Annealing of the quenched-in resistivity, $\Delta\rho_q$, in ErH_{2+x}, with $x=0.048$ and 0.054. The inset to the right gives the derivatives of the recovery curves, indicating the two peaks concerning the SRO and LRO processes, respectively.

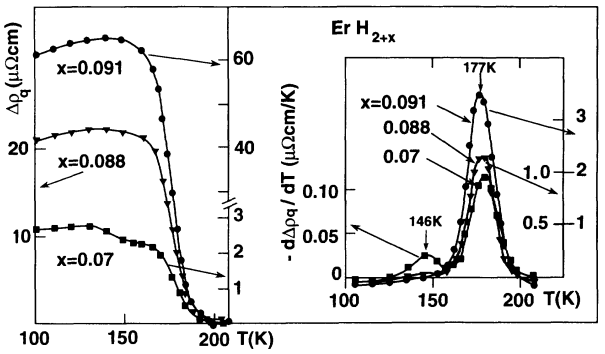

FIG. 4. Same as Fig. 3, for $x=0.07$, 0.088, and 0.091. Note the progressive disappearance of the SRO process with growing x.

the x atoms and results in a residual-resistivity increase, which is a function of the (disordered) x concentration as seen in Figs. 1 and 2. Annealing of the quenched specimens shows that the introduced $\Delta\rho_q$ recovers in the anomaly region, i.e., in the temperature range where the frozen-in x hydrogens become mobile enough to form the ordered configuration, just before breaking up again at somewhat higher T.

One can analyze the recovery kinetics of the frozen-in "defects" in the H_0 sublattice and determine their activation energy for migration E_m, assuming a first-order single activated process, from

$$E_m = kT_p^2[\Delta\rho_q(T_p)]^{-1} d\Delta\rho_q(T_p)/dT \ , \tag{1}$$

by measuring the annealed $\Delta\rho_q$ and its derivative at the peak temperature T_p (for details, see, e.g., Ref. 15). We have performed such an analysis for all specimens exhibiting a structural anomaly and show in Figs. 3–6 examples of typical behavior.

Thus, in Fig. 3, where the data for $x=0.048$ and 0.054 are presented, the immediately striking observation is the fact that the quenched-in resistivity of the former sample recovers in one simple stage, while the recovery of the latter takes place in two stages. The low-T stage, common for both specimens, occurs at $T_p^{(1)}=141$ K; the high-T stage, is only seen for $x=0.054$, at $T_p^{(2)}=177$ K.

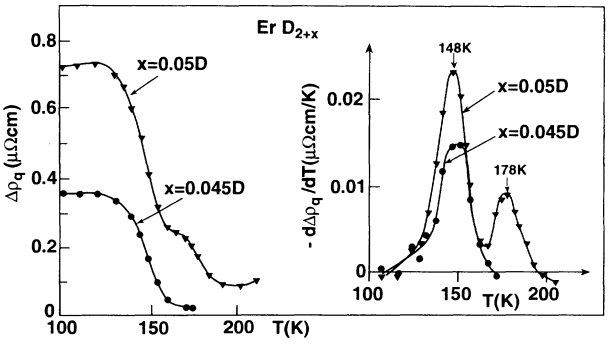

FIG. 5. Annealing of the quenched-in $\Delta\rho_q$ in ErD_{2+x}, with $x=0.045$D and 0.05D. Note the beginning LRO process for $x=0.05$D peaking at 178 K.

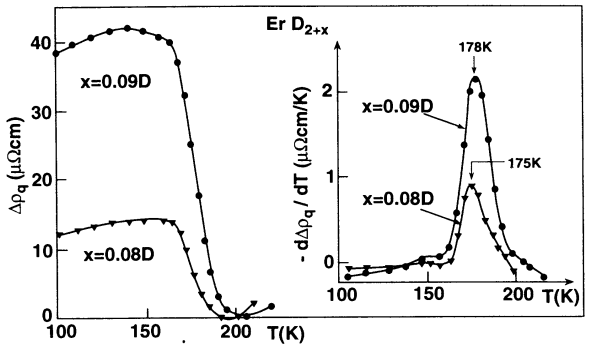

FIG. 6. Same as Fig. 5, for $x=0.08$D and 0.09D, with hardly observable SRO-type recovery.

The respective activation energies, determined according to Eq. (1), are $E_m^{(1)}=0.185\pm0.01$ eV and $E_m^{(2)}=0.31(1)$ eV. It is tempting, in analogy with other RH_{2+x} systems, to assign the former process to short-range ordering (SRO) and the latter to long-range ordering (LRO) of the x hydrogens. It is noteworthy that the addition of just 0.006 at.%H/at.%Er to the $x=0.048$ sample is enough to induce a sufficient interaction between the x atoms in the H_0 sublattice of the LRO to emerge and to coexist with SRO in a roughly equal proportion. Going over to higher concentrations (Fig. 4), we mark the progressive disappearance of the SRO stage, which still makes up $\sim20\%$ of the total in the case of $x=0.07$, but leaves only LRO for the two x-richest samples. The activation energies for the two processes are $E_m^{(1)}=0.18$ eV and $E_m^{(2)}=0.29$–0.30 eV, respectively.

Quenching of the deuterides has a qualitatively similar effect. In Fig. 5 are presented the recovery curves for $x=0.045$ D and $x=0.05$ D. Again, one notes the emergence of the LRO stage for the $x=0.05$D specimen, where it is responsible for $\sim\frac{1}{4}$ of the total recovery. The temperatures for the SRO stage, $T_p^{(1)}=148$–149 K, are somewhat higher than for the comparable ErH_{2+x} specimens, while the LRO stage shows practically no isotope effect. The activation energies are also quite the same as for the respective hydrides: $E_m^{(1)}=0.16$–0.17 eV and $E_m^{(2)}=0.30(1)$ eV. The x-richer specimens $x=0.08$ D and $x=0.09$ D (Fig. 6) exhibit practically only the LRO stage, with just a few percent of SRO remaining and recognizable as a vague shoulder around 150 K.

To summarize this subsection, we have collected the data concerning E_m and T_p for all measured $ErH(D)_{2+x}$ specimens in Fig. 7 as a function of x. The upper part shows the activation energies for both ordering processes; within the measuring precision, there is no isotope effect on either E_m(SRO) or E_m(LRO). But, while the former is practically constant within the x range of existence, the latter exhibits a slightly decreasing tendency with increasing x, in agreement with our earlier measurements on β-PrH_{2+x} (Ref. 16) and also with the nuclear-magnetic-resonance measurements on β-LaH_{2+x} (Ref. 17). Here, the increasing mobility with x could be related, via the higher resistivity and increasing ionicity of the

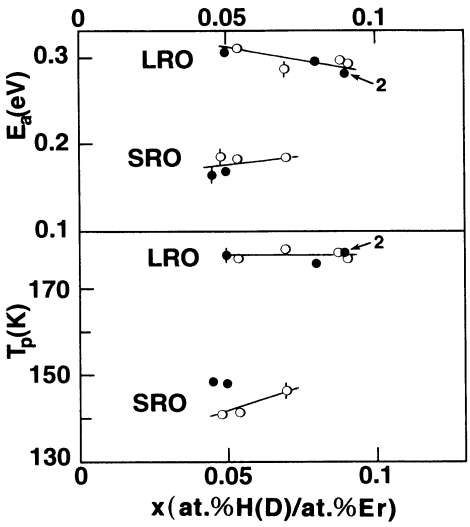

FIG. 7. Upper part; activation energies for migration of the quenched-in $H(D)_0$ species for the SRO and for the LRO processes. Lower part: peak temperatures for the SRO and LRO processes, respectively. (○): H (●): D.

samples, to a lowering of the potential barrier for diffusional jumps. The peak temperature T_p (lower part of Fig. 7), however, is independent of x for the LRO process and seems slightly increasing (just one value) for SRO; one notes, on the other hand, a clear isotope effect for $T_p^{(1)}$ of the SRO process (7–8° higher for D), which indicates, in view of the constant or even somewhat lower E_m(SRO), a lower jump frequency for the D_0 atoms when compared to the H_0 mobility.

Finally, we present in Fig. 8 the resistivity isothermal

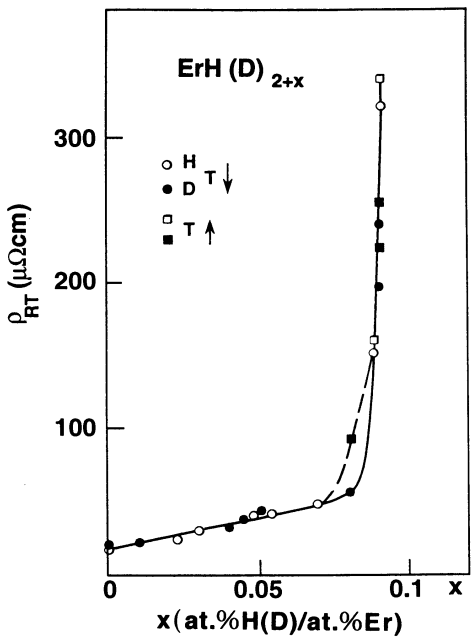

FIG. 8. Resistivity isothermal at room temperatures as a function of x for all measured $ErH(D)_{2+x}$ specimens, diverging near the β-phase limit. (○,□): H, (●,■): D, taken with decreasing or with increasing temperature.

at room temperature for all specimens, taken with increasing and with decreasing T, which shows the hysteresis effect of the LRO specimens near the order-disorder transformation. The ρ increase is practically linear with x until $x \sim 0.07$, from where it diverges in a superexponential way, indicating the limit of the pure β phase near $x = 0.09$, probably with the appearance of insulating γ-phase germs. This conforms with the difficulty encountered during the hydrogenation to prepare stable specimens with higher concentrations and also with the observation of differing H-absorption kinetics in these cases. Similar divergent ρ isothermals had been noted before on YH_{2+x} (Ref. 4) and on NdH_{2+x} (Ref. 18) when approaching the β-phase limit.

B. Magnetic ordering

At low temperature, the $ErH(D)_{2+x}$ specimens exhibit magnetic transitions as shown in Figs. 9 and 10. The resistivity of the pure dihydride, $x = 0$, possesses an angular point at $T_N = 2.32(2)$ K, and that of the dideuteride (not shown here) at $T_N = 2.35(2)$ K; the difference between the two is at the limit to the measuring precision, though it seems confirmed in the susceptibility studies of Ref. 13, with $T_N(ErH_2) = 2.30(5)$ K and $T_N(ErD_2) = 2.36(5)$ K. In principle, as no isotope effect is expected in the magnetic properties, we prefer to attribute the slightly lower T_N of the dihydride to a contamination by ≤ 0.001 at. %H/at. %Er on O sites, which, by the way, could also explain its somewhat higher residual resistivity by ~ 0.1 $\mu\Omega$ cm. The above value for T_N should be compared with the $T_N = 2.4(1)$ K obtained in Mössbauer measurements,[8] the 2.13(3) K in specific heat,[7] and the 2.15(5) K in neutron diffraction.[10] The slightly lower T_N in the two latter experiments could have a similar contaminational origin as the "isotope effect" above. An important result is the confirmation of the observation of only one magnetic transition in $ErH(D)_2$, at least down to 1.3 K, in contrast to the two transitions measured in pure Tb, Dy, and Ho dihydrides,[5,10,19–21] indicating the presence of an intermediate incommensurate (IC) structure before the emergence of the commensurate antiferromagnetic (AF) configuration. In ErD_2, Shaked *et al.*[10] had suggested the simultaneous presence of both the commensurate and the IC components down to 1.4 K, implying a possible vanishing of the latter for even lower T. The existence of an overlap region between the two magnetic phases is not improbable and similar effects have bene noted in $TbH(D)_2$.[21] Neutron-diffraction measurements to lower temperatures, preferably below 1 K, are, thus, highly desirable.

Adding x hydrogens to the pure dihydride (Fig. 9) reduces first the value of T_N, yielding $T_N = 1.85$ K for $x = 0.03$ and 1.75 K for $x = 0.07$. At the same time, the resistivity exhibits a flat minimum at 12–15 K before peaking or breaking at T_N. For still higher H_0 concentrations, $x = 0.088$, a resistivity decrease (with *decreasing* T) at the lowest measured temperatures is no longer observed and T_N cannot be defined as easily. In Fig. 10 we have, therefore, plotted the resistivity derivatives for specimens with higher values of x and note additional structures at 2.1–2.2 K. Similar ρ minima had been noted earlier in other superstoichiometric dihydrides, e.g., in $GdH(D)_{2+x}$ (Ref. 22), $TbH(D)_{2+x}$ (Ref. 19), DyH_{2+x}

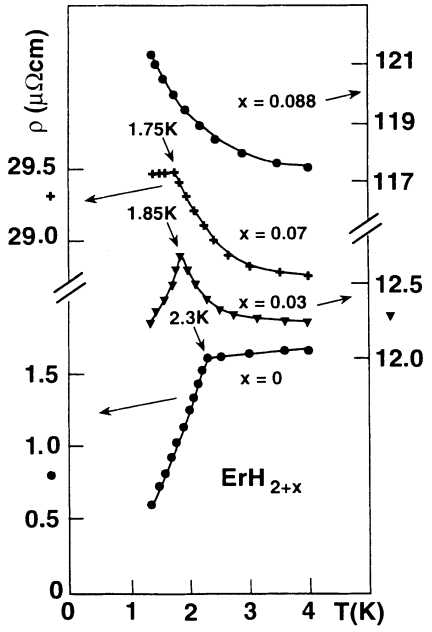

FIG. 9. Resistivity in the magnetic region of several ErH_{2+x} specimens, with $0 \leq x \leq 0.088$, showing the transition temperatures T_N.

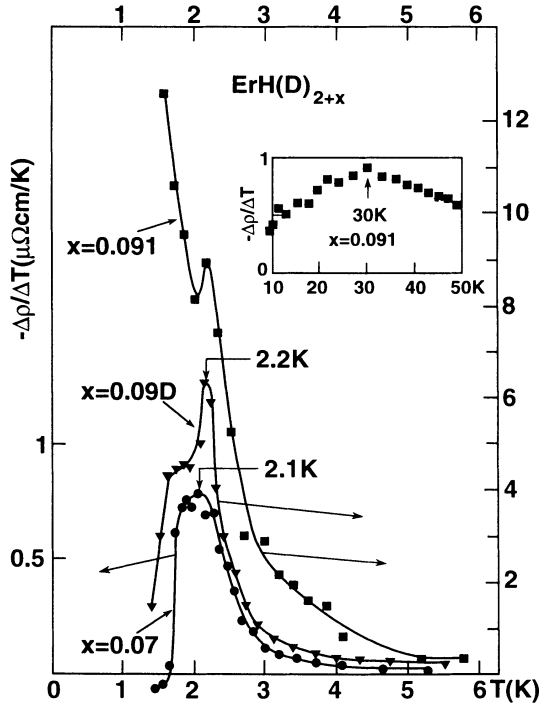

FIG. 10. Resistivity derivatives in the magnetic region for x-rich $ErH(D)_{2+x}$-specimens: $x = 0.07$, 0.09D and 0.091. The special points correspond to magnetic transitions. The inset shows an additional $d\rho/dT$ maximum of the $x = 0.091$ sample near 30 K.

(Ref. 20), SmH_{2+x} (Ref. 23), and were associated with the opening of new gaps in the magnon spectrum due to IC ordering or to magnetic fluctuations (magnetic SRO). On the other hand, minima in the pure dihydrides PrH_2 (Ref. 24) and HoH_2 (Ref. 5) were attributed to transitions from a magnetic ground state to a nonmagnetic first excited state, which is not the case here in ErH_2.

Finally, we show in the inset of Fig. 10 a further anomaly near 30 K for the x-richest specimen, $x=0.091$, which is also seen in Fig. 1 in the form of a bump superimposed upon the low-T resistivity decrease. Its origin is not clear for the present, but it reminds one of similar manifestations in other RH_{2+x} systems[19–22] for high x values, where the perturbation of the CF symmetry by the ordering in the H_0 sublattice is strong enough to induce eventually new magnetic transitions or at least contributions to spin-disorder scattering. It is typical for such a mechanism that the quenched $x=0.091$ specimen (uppermost Q curve in Fig. 1) should exhibit a smaller (flatter) bump than the relaxed one (R) if the ordering state of the H_0 sublattice is involved.

Concluding this subsection we propose a tentative magnetic phase diagram (Fig. 11) in the system $ErH(D)_{2+x}$ through the pure β phase, $0\le x\le 0.09$, where we peruse all present electrical-resistivity data together with the magnetic-susceptibility data from Refs. 9 and 13, and the neutron-diffraction result of Shaked *et al.*[10] As discussed above, the low-T phases are mixed, consisting of commensurate and IC components, followed at small x values by a SRO region. For $x\ge 0.05$, the appearance of a LRO structural configuration in the H_0 sublattice (see Sec. III A is accompanied by a new (probably IC) magnetic phase, which itself is followed by a magnetic fluctuation region before turning paramagnetic. (The 30 K bump has not been considered.) The latter remains to be confirmed by neutron diffraction, but seems reasonable in view of what is known from other heavy RH_{2+x} systems. It has been clearly demonstrated in the case of $TbH(D)_{2+x}$, where H sublattice ordering for

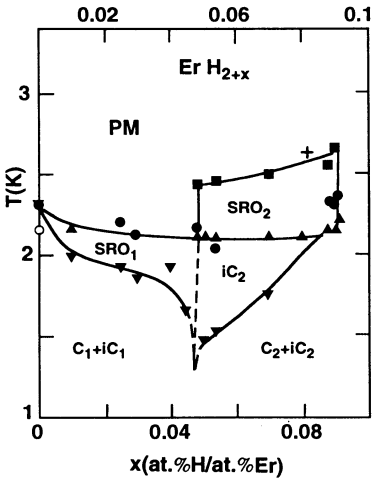

FIG. 11. Tentative magnetic phase diagram constructed from the present resistivity data (▼,▲), together with the susceptibility data from Refs. 9(+) and 13(●,■), and from neutron diffraction (Ref. 10) (○).

$x\ge 0.15$, as determined through neutron scattering,[14] induced new commensurate and IC magnetic phases.[21]

C. Metal-semiconductor transitions

We have seen in Figs. 1 and 2 that the specimens with the highest x concentrations undergo a metal-semiconductor transition with increasing temperature in the region 240–290 K and another one at low temperature (LT), with decreasing T. The latter is rather flat and less well defined because of interfering magnetic fluctuations, in particular, in the case of the less resistive samples, $x=0.08$D and 0.088, while the extremal $x=0.091$ specimen exhibits a very deep and impressive minimum at 100–120 K—high enough not to involve any magnetic effects. An important phenomenon are the strong hysteresis effects, the transition temperature T_{MS} being higher by 10–30° in a warming-up regime than when cooling down. Furthermore, the specimens seem to be in a relatively unstable state, repeated cooling-heating cycles and especially a quench across the LRO stage region around 200 K led to increasing sample resistivity, even after annealing of the quenched-in $\Delta\rho_q$.

As in the case of YH_{2+x} (Ref. 4), with $x=0.095$–0.10, we attribute the MS transition to the breakdown of a delocalized carrier band situated near the Fermi level when increasing the temperature. This band is related to the LRO configuration of the H_0 atoms and forms together with the ordered structure in the H_0 sublattice with decreasing temperature below ~200 K, due to the newly acquired structural periodicity. The model follows that proposed by Shinar *et al.*[3,25] for the MS transition in substoichiometric trihydrides LaH_{3-x} where the ordering occurred in the V_0 sublattice of the octahedral vacancies, in contrast to that in the direct H_0 sublattice of our case. Upon heating, the ordered configuration collapses followed by the breakdown of the delocalized band, which leads to the opening of a gap. One can determine its width Δ by plotting the resistivity in an Arrhenius graph,

$$\ln\rho \propto E_a/kT\ , \tag{2}$$

which is shown for the two specimens $x=0.09$D and 0.091, both in the relaxed and in the quenched state, in Fig. 12. The effective activation energies across the gap, $E_a=\Delta/2$, are measured as the high-T slopes in Fig. 12:

$$E_a(x=0.09\text{D})=58(10)\ \text{meV}\ ,$$

$$E_a(x=0.091)=40(10)\ \text{meV}\ ,$$

slightly higher but of the same order of magnitude as the 15–20 meV of the YH_{2+x} specimens of Ref. 4.

As concerns the LT-MS transition, we are tempted to assign it to carrier localization caused by atomic disorder due to the presence of the octahedral hydrogens. We have analyzed our results in terms of the variable-range-hopping (VRH) mechanism of Mott[26] and obtained a good fit, using for the resistivity, a form with a preexponential factor,

$$\rho=\rho_0(T/T_0)^{1/2}\exp(T_0/T)^{1/4}\ . \tag{3}$$

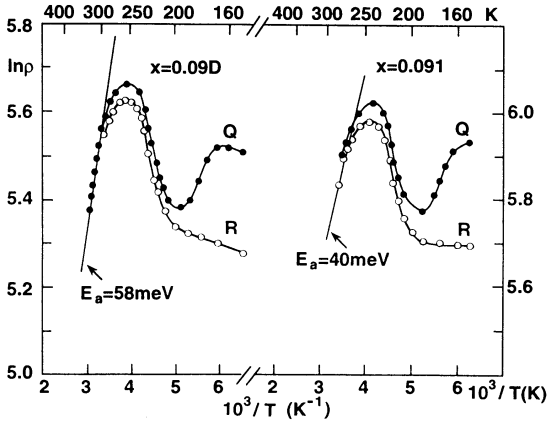

FIG. 12. Arrhenius graphs for $x=0.09$D (to the left) and $x=0.091$ (to the right) in the relaxed (R) and in the quenched (Q) states, giving the effective activation energies E_a in the semiconducting region at the high-temperature side of the MS transition.

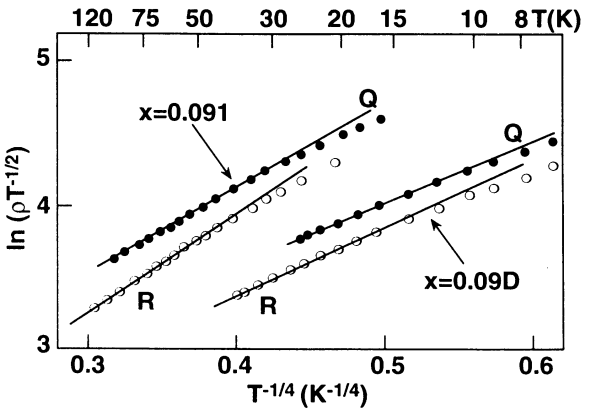

FIG. 13. The resistivities at the low-T side of the SM transition for the specimens of Fig. 12, plotted as $\ln(\rho/\sqrt{T})=f(T^{-1/4})$.

The weakly temperature-dependent prefactor is suggested through the role played by inelastic-scattering events due to phonons, for $T>\Theta_D$, or by magnons, for $T>T_N$; in the present case of a magnetically active system, we prefer the latter mechanism, since the former would give a too high T region of validity for the Debye temperatures involved, $\Theta_D\approx 380$ K.[1] (An exhaustive discussion of the behavior around a MS transition has been recently given by Abkemeier *et al.*[27] who applied it to Si-Ni alloys, and by Mustefa, Boutiche, and Khodja.[28] Further successful applications were made in the case of high-T_c superconducting ceramics, e.g., by Kastner *et al.*[29] and Osquiguil *et al.*[30]) Figure 13 shows the fitting of expression (3) to the experimental data concerning the same specimens with $x=0.09$D and $x=0.091$ in the R state and in the Q state as in Fig. 12. We obtain for the fitting parameters ρ_0 and T_0,the following values:

$$x=0.09\text{D}:\ \text{R}-\rho_0=100\ \mu\Omega\,\text{cm},\ T_0=430\ \text{K},$$
$$\text{Q}-\rho_0=115\ \mu\Omega\,\text{cm},\ T_0=320\ \text{K},$$
$$x=0.091:\ \text{R}-\rho_0=155\ \mu\Omega\,\text{cm},\ T_0=1975\ \text{K},$$
$$\text{Q}-\rho_0=200\ \mu\Omega\,\text{cm},\ T_0=1090\ \text{K}.$$

As already discussed in the Introduction, the connection between structural order-disorder transformation and the MS transition was noted as early as 1972 by Libowitz, Pack, and Binnie,[2] who related the latter with the cubic-to-tetragonal distortion in the metal lattice observed in $CeH_{2.7}$ at low temperatures. This problem was later treated theoretically by Fujimori and Tsuda,[31] who calculated the electronic structure of CeH_{2+x} with $0\le x\le 1$, and showed that defect levels due to octahedral vacancies V_0 acted as donors and formed a band under certain conditions. These ideas were used by Shinar *et al.*[25] to interpret their results on the observation of MS transitions in LaH_{3-x}.[3] The theoretical situation seems, however, not completely satisfactory, as a recent systematic study of the electronic structure of YH_3,[32] using the self-consistent localized spherical wave method, has not revealed any gap, neither in the fcc nor in the hcp structure. A further interesting experimental correlation between structural changes and a metal-insulator transition was noted recently in the $R\text{NiO}_3$ (R = La, Pr, Nd, Sm) system,[33] suggesting coupled tilts of NiO_6 octahedra accompanying the electronic localization. On the other hand, in a treatment of hole movement in an antiferromagnetically correlated matrix, Kumar[34] found that isolated holes are localized at discrete levels, while incipient pairing can lead to delocalization with metallic conduction.

In our case of relatively low x concentrations, the ordering (for $x\gtrsim 0.05$) occurs in the direct H_0 sublattice, and the defect levels correspond to the s electrons of the H_0 atoms which are found in isolated states below the d band. At low temperatures, the periodicity of the newly formed ordered configuration is then responsible for their condensation into a delocalized defect band and the crystal becomes a metallic conductor. The fact that the MS transitions are only observed for concentrations $x\gtrsim 0.09$, i.e., higher than the $x_{\text{LRO}}\sim 0.05$ where LRO begins to

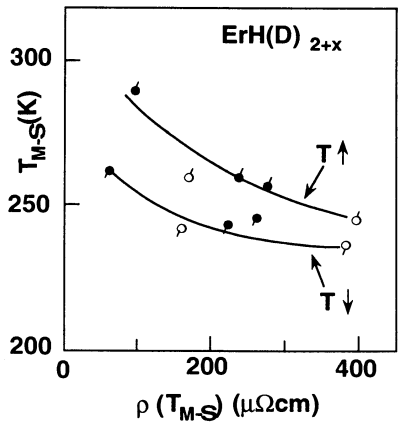

FIG. 14. Temperature of the MS transition as a function of the resistivity at this temperature. (○): H, (●): D.

appear, seems to be conditioned by the additional requirement of having a sufficiently low carrier density, which occurs just at the limit of the pure β phase: ~ 0.09 at H/Er. In this context, it is interesting to note that the transition temperatures T_{MS} are the lower, the more resistive the specimens. In Fig. 14 we have shown this direct relationship between T_{MS} and the resistivity value at T_{MS} for all transforming specimens, indicating an increasing stability of the delocalized band with increasing carrier density. The absence of a detectable isotope effect is a further sign for a purely electronic mechanism for the MS transition itself, though indirectly driven by a structural transformation.

IV. CONCLUSIONS

Like other RH_{2+x} systems, $ErH(D)_{2+x}$ exhibits structural ordering in the octahedral H_0 sublattice of the excess hydrogen atoms x, which begins slightly below $x \sim 0.05$ at. %H(D)/at. %Er as SRO and transforms into LRO for $x \gtrsim 0.05$, coexisting with the former until $x \sim 0.07$. The similarity of its behavior under quench, especially the recovery temperatures and activation energies for migration of the x atoms, makes it plausible to assume a DO_{22} structure for its configuration as in TbD_{2+x}, analyzed earlier.

The structural ordering interacts with the magnetism of the hydride via the CF or the Fermi surface, leading to new magnetic behavior for $x \gtrsim 0.05$; for lower x concentrations, the magnetic transition temperatures T_N diminish regularly due to the decreasing mediating carrier density according to Ruderman-Kittel-Kasuya-Yosida (RKKY) interaction.

Finally, the order-disorder transformation of the H_0 sublattice at $\sim 200-250$ K is responsible for a MS transition occurring at the end of it, if the carrier density in the sample is low enough, i.e., for x close to the β-phase limit. Another (LT) MS transition, occurring in the same specimens at $\sim 40-120$ K, can be described by carrier localization through a Mott mechanism.

---

*Deceased.

[1] P. Vajda and J. N. Daou, in *Hydrogen-Metal Systems,* edited by A Aladjem and F. A. Lewis (VCH, Weinheim, Germany, in press), Vol. I, Chap. 3a.

[2] G. G. Libowitz, J. G. Pack, and W. P. Binnie, Phys. Rev. B **6**, 4540 (1972).

[3] J. Shinar, B. Dehner, B. J. Beaudry, and D. T. Peterson, Phys. Rev. B **37**, 2066 (1988).

[4] P. Vajda and J. N. Daou, Phys. Rev. Lett. **66**, 3176 (1991); J. N. Daou and P. Vajda, Phys. Rev. B **45**, 10 907 (1992).

[5] P. Vajda and J. N. Daou, Z. Phys. Chem. **179**, 403 (1993).

[6] Y. Kubota and W. E. Wallace, J. Chem. Phys. **39**, 1285 (1963).

[7] J. Opyrchal and Z. Bieganski, Solid State Commun. **20**, 261 (1976).

[8] G. K. Shenoy, B. D. Dunlap, D. G. Westlake, and A. E. Dwight, Phys. Rev. B **14**, 41 (1976).

[9] R. L. Carlin and L. J. Krause, Phys. Rev. B **23**, 6149 (1981).

[10] H. Shaked, D. G. Westlake, J. Faber, and M. H. Mueller, Phys. Rev. B **30**, 328 (1984).

[11] J. N. Daou, P. Vajda, and J. P. Burger, Phys. Rev. B **37**, 5236 (1988).

[12] J. P. Burger, J. N. Daou, P. Vajda, and A. Lucasson, J. Less-Common Met. **103**, 381 (1984).

[13] A. Boukraa, P. Vajda, and J. N. Daou, J. Magn. Magn. Mater. **123**, L5 (1993).

[14] G. André, O. Blaschko, W. Schwarz, J. N. Daou, and P. Vajda, Phys. Rev. B **46**, 8644 (1992).

[15] J. N. Daou, P. Vajda, J. P. Burger, and A. Lucasson, Phys. Status Solidi A **98**, 183 (1986).

[16] J. P. Burger, J. N. Daou, and P. Vajda, Philos. Mag. B **58**, 349 (1988).

[17] D. S. Schreiber and R. M. Cotts, Phys. Rev. **131**, 1118 (1963).

[18] J. N. Daou, J. P. Burger, and P. Vajda, Philos. Mag. B **65**, 127 (1992).

[19] P. Vajda, J. N. Daou, and J. P. Burger, Phys. Rev. B **36**, 8669 (1987).

[20] P. Vajda and J. N. Daou, Phys. Rev. B **45**, 9749 (1992).

[21] P. Vajda, J. N. Daou, and G. André, Phys. Rev. B **48**, 6116 (1993).

[22] P. Vajda, J. N. Daou, and J. P. Burger, J. Less-Common Met. **172-174**, 271 (1991).

[23] P. Vajda, J. N. Daou, and J. P. Burger, Phys. Rev. B **40**, 500 (1989).

[24] J. P. Burger, J. N. Daou, and P. Vajda, Z. Phys. B **80**, 233 (1990).

[25] J. Shinar, B. Dehner, R. G. Barnes, and B. J. Beaudry, Phys. Rev. Lett. **64**, 563 (1990).

[26] N. F. Mott and E. A. Davis, *Electronic Processes in Non-Crystalline Materials* (Clarendon, Oxford, 1979).

[27] K. M. Abkemeier, C. J. Adkins, R. Asal, and E. A .Davis, J. Phys. Condens. Matter. **4**, 9113 (1992).

[28] M. Mostefa, S. Boutiche, and M. Khodja, Solid State Commun. **82**, 697 (1992).

[29] M. A. Kastner, R. J. Birgeneau, C. Y. Chen, Y. M. Chiang, D. R. Gabbe, H. P. Jenssen, T. Junk, C. J. Peters, P. J. Picone, T. Thio, T. R. Thurston, and H. L. Tuller, Phys. Rev. B **37**, 111 (1988).

[30] E. J. Osquiguil, L. Civale, R. Decca, and F. de la Cruz, Phys. Rev. B **38**, 2840 (1988).

[31] A. Fujimori and N. Tsuda, J. Phys. C **14**, 1427 (1981).

[32] J. P. Dekker, J. van Ek, and A. Lodder, J. Phys. Condens. Matter **5**, 4805 (1993).

[33] J.L. Garcia-Munoz, J. Rodriguez-Carvajal, P. Lacorre, and J. B. Torrance, Phys. Rev. B **46**, 4414 (1992).

[34] N. Kumar, Phys. Rev. B **42**, 6138 (1990).